JOURNAL OF MATERIALS SCIENCE 15 (1980) 931–938

Stress distributions along a short fibre in fibre reinforced plastics

CHOON T. CHON*, C. T. SUN†
Engineering Mechanics Department, General Motors Research Laboratories, Warren, Michigan 48090, USA

This paper develops an analysis for predicting the normal stress and interfacial shearing stress distribution along a single reinforcing fibre of a randomly oriented chopped-fibre composite, such as sheet moulding compound (SMC), from a knowledge of the constituent properties and the length-to-diameter ratio of the fibres. The analysis is useful in analysing the tensile strength of SMC, and as a guide to increasing the tensile strength by altering the elastic characteristics. The model is based on a generalized shear-lag analysis. Numerical values of the normal stress and interfacial shearing stress are presented as functions of various parameters. It is observed that the maximum normal stress occurs at the middle of the fibre and the maximum shear stress occurs at the end. The analysis is restricted to loading which does not result in buckling of the fibre; i.e., axial loads on the fibre can be at most only slightly compressive.

List of symbols

a_f	Ratio of the fibre length to diameter (aspect ratio, l_f/d_f)
E_a	Young's modulus of the composite (defined in Equation 21)
E_f	Young's modulus of the fibre material
E_m	Young's modulus of the matrix material
G_f	Shear modulus of the fibre material
G_m	Shear modulus of the matrix material
l	Half the length of the matrix sheath which surrounds the fibre
l_f	Half of the length of the fibre
Q	Defined in Equation 14.
R	Ratio of the length of the fibre to the matrix in a representative volume element; a parameter $0 \leqslant R \leqslant [(1/V_f - 1)]$
r_a	Radius of the composite body (we assume $r_a \gg r_m, r_f$)
r_f	Radius of the fibre
r_m	Radius of the matrix sheath which surrounds the fibre
u_a	Displacement of the composite along the fibre direction
u_f	Displacement of the fibre along the fibre direction
V_f	Fibre volume fraction
(XYZ)	Co-ordinate system with Z-axis parallel to the direction of the applied load (Fig. 1a)
(xyz)	Co-ordinate system which is rotated by α about the X-axis (Fig. 1a)
$(\bar{x}\bar{y}\bar{z})$	Co-ordinate system which is rotated by θ about the z-axis (Fig. 1b)
α	Fibre orientation angle measured from the Z-axis
γ_m	Engineering shear strain in the matrix
η	Defined in Equation 8
θ	Polar angle measured from the x–z plane
ξ	Defined in Equation 9
σ	Applied normal stress
σ_a	Normal stress in the composite along the fibre axis
σ_f	Normal stress in the fibre along the fibre axis
σ_m	Normal stress in the matrix along the fibre axis
τ	Shear stress on the fibre–matrix interface

1. Introduction

The need to produce fuel-efficient vehicles at

* Present address: Ford Motor Company, Metallurgy Department, Dearborn, Michigan 48121, USA.
† Present address: Department of Engineering Sciences, University of Florida, Gainesville, Florida 32611, USA

0022–2461/80/040931–08$02.80/0

reasonable cost has led the automotive industry to consider randomly oriented chopped-fibre reinforced plastics as a near-term substitute for steel in structural panels. The motivation for using chopped-fibre reinforced plastics (instead of continuous fibre composites) is two-fold: (1) the fabrication cost for chopped-fibre composite is considerably lower compared to that for continuous fibre composites, and (2) for mass production, chopped-fibre composites are more adaptable to certain moulding techniques as well as to the fabrication of complex shapes than are continuous-filament composites.

For design engineers, it is useful to know how the strength of this composite depends on its constituent properties and on the aspect ratio of the fibres. In order to calculate the strength of randomly oriented chopped fibre composites, it is first necessary to analyse the stress distribution along a fibre* – the objective of this paper.

We generalize a mathematical model based on a concept of shear-lag analysis [1]. The model consists of a cylindrical fibre surrounded by a sheath of resin†; the remainder of the surrounding material is assumed to exhibit average composite properties. In the "generalized" shear-lag analysis the direction of applied load makes an angle α with the direction of orientation of the fibres, while in the "original" analysis the load is parallel to the fibres. By assuming that the normal stress in the resin is negligible compared to the normal stress in the fibre, we obtain the normal stress of the fibre, σ_f, and the interfacial shear stress, τ, between the fibre and the resin. The more detailed analysis is developed in the next section.

Numerical calculations of σ_f and τ for sheet moulding compound (SMC) are presented as functions of fibre axial co-ordinate position, z, fibre orientation angle, α, and fibre volume fraction, V_f. We also present the results of maximum σ_f and τ for other composites such as glass–epoxy, graphite–epoxy, boron–epoxy and boron–aluminium. Important influences of each parameter on the distribution of σ_f and τ are discussed in detail.

2. Generalized shear-lag analysis

The basic idea of shear-lag analysis for composite materials was outlined in the previous section. We develop the more detailed analysis in this section.

2.1. Mathematical model

Based on the original shear-lag analysis [1], we start with the following model. A fibre is surrounded by matrix which is in turn surrounded by the composite material. A typical representative volume element is shown in Fig. 1a. By representative volume element, we mean the "smallest unit" in a macroscopic scale.

2.2. Basic assumptions

The assumptions in this analysis are:

(a) the bonding between the fibre and the matrix at the interface is perfect;

(b) along the fibre direction, the normal stress in the matrix is much smaller than the normal

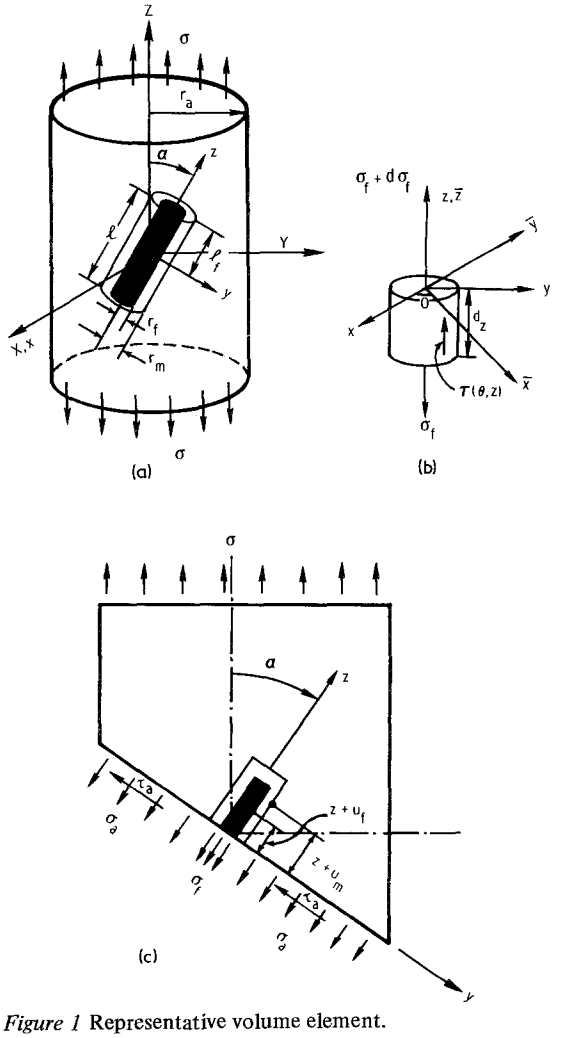

Figure 1 Representative volume element.

* The authors recognize that in fact, in practice, the fibres may appear as bundles rather than as individual fibres. However, the analytical approach described in this paper can be used for both types of reinforcement.

† In SMC, the glass fibres are more ribbon-like in cross-section, and adjacent fibres may actually contact each other where they cross. For the moment, we neglect these effects.

stress in the fibre, i.e. $|\sigma_m| \ll |\sigma_f|$ along the fibre direction;

(c) load is transmitted by the matrix material through interfacial shearing stress;

(d) the fibre does not buckle;

(e) adjacent ("nearest neighbour") fibres do not significantly disturb the stress field along the matrix sheath.

2.3. Analysis

The stresses on an element of fibre of length dz are shown in Fig. 1b. From equilibrium, we have

$$\int_0^{2\pi} \tau \, d\theta + \pi r_f \frac{d\sigma_f}{dz} = 0, \tag{1}$$

where σ_f is assumed to be independent of θ and r. The assumption of σ_f being independent of θ and r is reasonable for fibres with large ratio l_f/d_f, and when the fibre volume fraction is sufficiently small so that the portion of the fibre length which other neighbouring fibres interact with is small.

From overall equilibrium along the z-direction of the composite element shown in Fig. 1c, we have

$$r_f^2 \sigma_f + \left(\frac{r_a^2}{\cos\alpha} - r_f^2\right)\sigma_a = \sigma r_a^2 \cos\alpha. \tag{2}$$

The shear strain, γ_m, in the matrix is determined from the displacements of the fibre and the composite material. As shown in Fig. 1c, we have

$$u_a - u_f = \gamma_m (r_m - r_f). \tag{3}$$

Taking the first derivative of Equation 3 with respect to z and using the strain–displacement relations and the stress–strain relations, we obtain

$$\frac{1}{E_a}\sigma_a - \frac{1}{E_f}\sigma_f = \frac{r_m - r_f}{G_m}\frac{d\tau}{dz}, \tag{4}$$

where the average modulus of the composite, E_a, can be found either from experiment or from a knowledge of the constituent properties and the length-to-diameter ratio of the fibres [2–4]. From Equation 4, because σ_a and σ_f are independent of θ, we note that $d\tau/dz$ is also independent of θ. Therefore, we can write

$$\int_0^{2\pi} \frac{d\tau}{dz} d\theta = 2\pi \frac{d\tau}{dz}. \tag{5}$$

Substitution of Equation 5 into Equation 1 leads to

$$\frac{d\tau}{dz} + \frac{r_f}{2}\frac{d^2\sigma_f}{dz^2} = 0. \tag{6}$$

After combining Equations 2, 4 and 5, we finally obtain the following differential equation for σ_f,

$$\frac{d^2\sigma_f}{dz^2} - \eta^2 \sigma_f = -\xi^2 \tag{7}$$

where

$$\eta^2 = \frac{2G_m}{(r_m - r_f)r_f}\left[\frac{r_f^2 \cos\alpha}{E_a(r_a^2 - r_f^2\cos\alpha)} + \frac{1}{E_f}\right] \tag{8}$$

and

$$\xi^2 = \frac{2\sigma G_m r_a^2 \cos^2\alpha}{E_a r_f (r_m - r_f)(r_a^2 - r_f^2\cos\alpha)} \tag{9}$$

If we consider $r_f \ll r_a$*, we can then write Equations 8 and 9 as

$$\eta^2 = \frac{2G_m}{E_f(r_m - r_f)r_f} \tag{8a}$$

$$\xi^2 = \frac{2\sigma G_m \cos^2\alpha}{E_a r_f (r_m - r_f)}. \tag{9a}$$

The solution of Equation 7 is of the form

$$\sigma_f = A \sinh\eta z + B\cosh\eta z + \frac{\xi^2}{\eta^2}. \tag{10}$$

From assumption (b), the boundary conditions for σ_f are

$$\sigma_f(l_f) = \sigma_f(-l_f) = 0. \tag{11}$$

Substituting Equation 11 into Equation 10, we get

$$\sigma_f = \sigma\cos^2\alpha\left(\frac{E_f}{E_a}\right)\left(1 - \frac{\cosh\eta z}{\cosh\eta l_f}\right). \tag{12}$$

To determine τ, we substitute Equation 12 into Equation 6, and solve the resulting differential equation with the following result:

$$\tau = Q\sinh\eta z + C \tag{13}$$

where

$$Q = \frac{G_m\xi^2}{\eta^3(r_m - r_f)\cosh\eta l_f}\left[\frac{r_f^2\cos\alpha}{E_a(r_a^2 - r_f^2\cos\alpha)} + \frac{1}{E_f}\right] \tag{14}$$

or for $r_f \ll r_a$,

$$Q = \frac{G_m\xi^2}{E_f\eta^3(r_m - r_f)\cosh\eta l_f}. \tag{14a}$$

To evaluate the constant C, let us first observe that, in the original shear-lag analysis [1], $\tau = 0$ at the middle surface $z = 0$. In our present case,

* This applies in regions away from fibre-crossing points.

this situation is no longer generally true due to fibre inclination. The boundary condition for τ, however, at $z = 0$ is shown in Appendix 1 to be

$$\tau = -\sigma \sin\alpha \cos\alpha \sin\theta. \quad (15)$$

Thus, the complete solution for τ can be obtained as

$$\tau = Q \sinh \eta z - \sigma \sin\alpha \cos\alpha \sin\theta, \quad (16)$$

after we substitute Equation 15 into Equation 13. We choose the boundary condition for τ which gives

$$\int_0^{2\pi} \tau \, d\theta = 0 \quad (17)$$

at $z = 0$ in order to satisfy Equation 1, since $d\sigma_f/dz$ vanishes at $z = 0$ from Equation 12.

3. Results and discussions

Before proceeding it is convenient to introduce the following parameters:

$$a_f = \frac{l_f}{d_f}, \qquad V_f = \frac{r_f^2 l_f}{r_m^2 l}, \qquad R = \frac{l - l_f}{l_f}, \quad (18)$$

where a_f is the (aspect) ratio of the fibre length to its diameter, V_f is the volume fraction of the fibre and R is the parameter which measures the ratio of the length of the fibre and the matrix in a representative volume element. Then we can express

$$\eta l_f = a_f \left[\frac{2G_m/E_f}{(1/\sqrt{[V_f(1+R)]} - 1)}\right]^{1/2} \quad (19)$$

and from Equation (14a)

$$Q = \frac{\sigma(\cos^2\alpha) G_m}{E_a\{(2G_m/E_f)(1/\sqrt{[V_f(1+R)]} - 1)\}^{1/2} \cosh \eta l_f}. \quad (20)$$

For Young's modulus of the composite, E_a, we use the formula proposed by Weng and Sun [3]. For the sake of brevity, we present only the final form here:

$$E_a = \frac{1}{\mu_1}(\mu_1^2 - \mu_2^2) \quad (21)$$

where

$$\mu_1 = (3/8)E_{11} + \frac{\mu_{12}}{2} + \frac{(3 + 2\nu_1 + 3\nu_1^2)\mu_{23}K_{23}}{2(\mu_{23} + K_{23})} \quad (22a)$$

$$\mu_2 = (1/8)E_{11} - \frac{\mu_{12}}{2} + \frac{(1 + 6\nu_1 + \nu_1^2)\mu_{23}K_{23}}{2(\mu_{23} + K_{23})} \quad (22b)$$

$$E_{11} = \frac{V_f E_f (1+R)^2}{1 + (E_f R/E_m)} + [1 - V_f(1+R)]E_m \quad (22c)$$

$$\mu_{12} = \left[\frac{G_f(1+V_f) + G_m(1-V_f)}{G_f(1-V_f) + G_m(1+V_f)}\right] G_m \quad (22d)$$

$$\mu_{23} = \left[1 + \frac{V_f}{\frac{G_m}{G_f - G_m} + \frac{(k_m + 7G_m/3)(1-V_f)}{2(k_m + 4G_m/3)}}\right] G_m \quad (22e)$$

$$\nu_1 = [1 - V_f(1+R)]\nu_m + V_f(1+R)\frac{\nu_f E_m + R\nu_m E_f}{RE_f + E_m} \quad (22f)$$

$$K_{23} = k_m + \frac{G_m}{3} + \frac{V_f}{\frac{1}{(k_f - k_m) + \frac{(G_f - G_m)}{3}} + \frac{1 - V_f}{k_m + 4G_m/3}} \quad (22g)$$

$$k_m = \frac{E_m}{3(1 - 2\nu_m)} \quad (22h)$$

$$k_f = \frac{E_f}{3(1 - 2\nu_f)} \quad (22i)$$

In Fig. 2, we plot σ_f/σ as a function of z/l_f using different values of α. The fibre volume

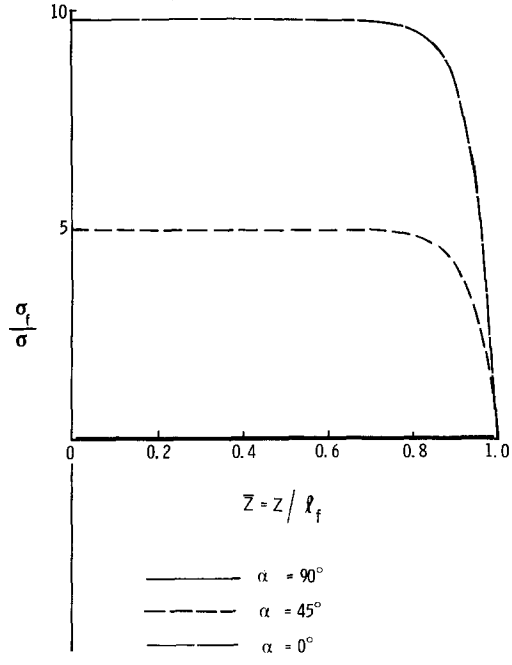

Figure 2 Plot of σ_f/σ as a function of z/l_f.

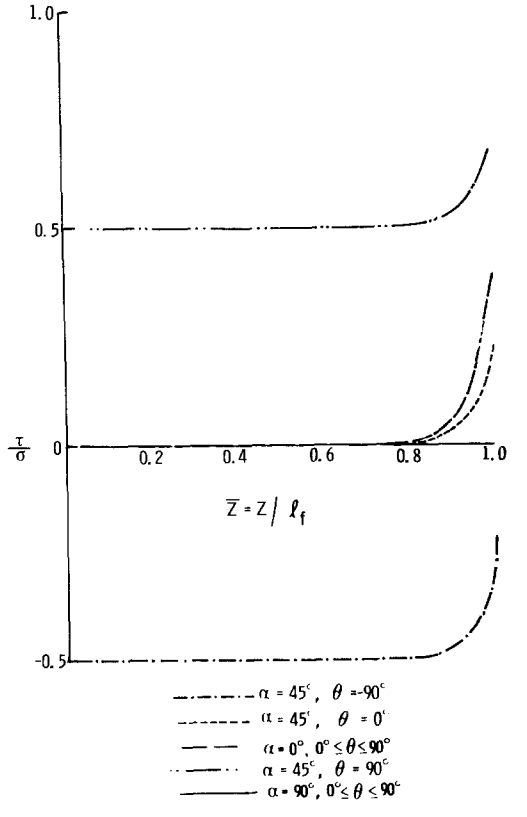

Figure 3 Plot of τ/σ as a function of z/l_f.

fraction, fibre aspect ratio and the constituent properties of the fibre and the matrix materials are assumed to be the same as those of SMC-30.* From Fig. 2, we observe that the maximum σ_f occurs at the mid-length of the fibre. The value of σ_f remains almost unchanged over the interval $0 \leqslant |z| \leqslant l_f$ and then changes rapidly to reach its minimum value at $|z| = l_f$.

In Fig. 3, we plot τ/σ as a function of z/l_f for SMC-30, using different values of α and θ. From Fig. 3, we observe that the maximum τ occurs at each end of the fibre. The value of τ remains almost unchanged over the interval $0 \leqslant |z| \leqslant l_f$ and then changes rapidly to reach its maximum value at $|z| = l_f$.

In Fig. 4, $\sigma_{f,max}$ ($z = 0$ and τ_{max} ($|z| = l_f$) are plotted as functions of the fibre aspect ratio, a_f. Again the composite material chosen in this plot is SMC-30. It is observed in Fig. 4 that a_f has little influence on τ_{max}, but the value of $\sigma_{f,max}$ strongly depends on the value of a_f over the range $0 \leqslant a_f \leqslant 50$. As a_f exceeds 50, $\sigma_{f,max}$ rapidly reaches its maximum value asymptotically. In Fig. 5, we plot $\sigma_{f,max}$ and τ_{max} as functions of fibre volume fraction for SMC composite. Both $\sigma_{f,max}$ and τ_{max} decrease as V_f increases. This is attributed to the fact that as V_f increases, more fibres will take part in carrying the applied load.

In Fig. 6, we plot σ_f as a function of fibre inclination angle, α, for SMC-30 using z as a parameter. It is seen in Fig. 6 that σ_f decreases as α increases from 0° to 90°.

In Fig. 7, we plot τ as a function of α for SMC-30 using z and θ as parameters. From Fig. 7, we observe that for $\theta = \pm 90°$, maximum values of τ occur in the region $30° \leqslant \alpha \leqslant 60°$ for all values of z, and for $\theta = 0°$ the maximum values of τ always occur at $\alpha = 0$. It is also interesting to note that the exact location of α in which τ reaches its maximum value depends on the value of z as well as on the geometry and the constituent material properties.

In Fig. 8, we plot $\sigma_{f,max}$ as a function of α for different composites such as boron–aluminium,

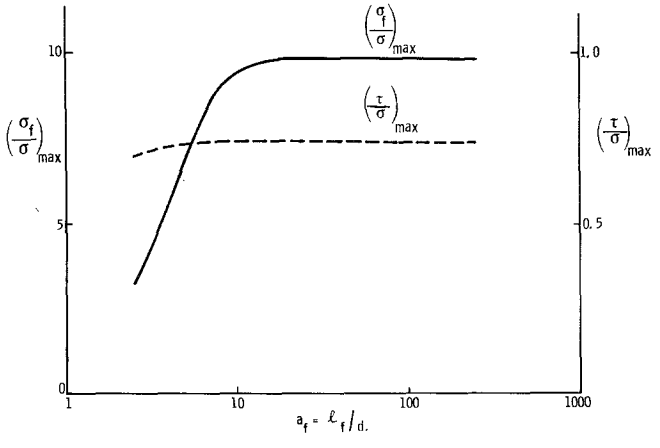

Figure 4 Plot of $\sigma_{f,max}$ and τ_{max} as a function of a_f.

* For detail see Appendix 2.

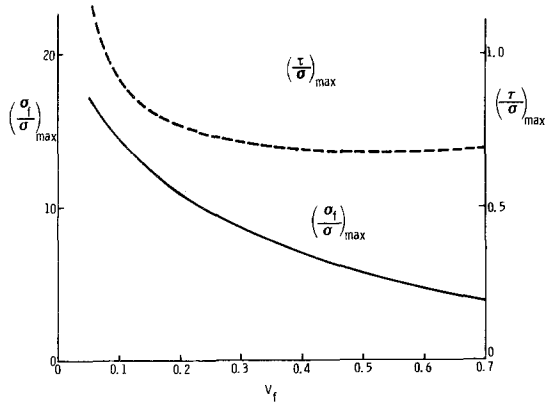

Figure 5 Plot of $\sigma_{f,max}$ and τ_{max} as a function of V_f.

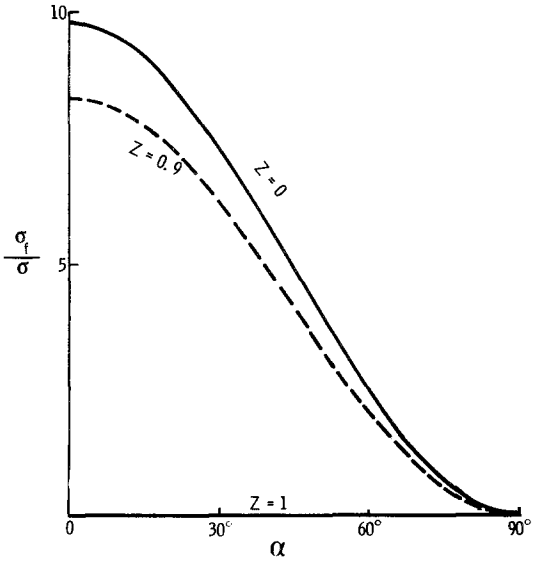

Figure 6 Plot of σ_f/σ for SMC-30 as a function of α.

boron–epoxy, SMC and graphite–epoxy. It is observed that the maximum value of $\sigma_{f,max}$ increases as the ratio E_f/G_m increases.

In Fig. 9, we plot τ_{max} as a function of α for the same composites. It is observed that the trend is just the opposite, i.e. the maximum value of τ_{max} increases as E_f/G_m decreases.

This latter observation can sometimes be used as a guide in altering the *elastic* characteristics of the constituents so as to increase the composite *strength*. Very simply, if the composite fails primarily as a result of *fibre breakage*, *decrease* E_f/G_m (by modifying the matrix – changing its composition to make it stiffer or increasing the percentage of filler*) so as to decrease σ_f. If it fails

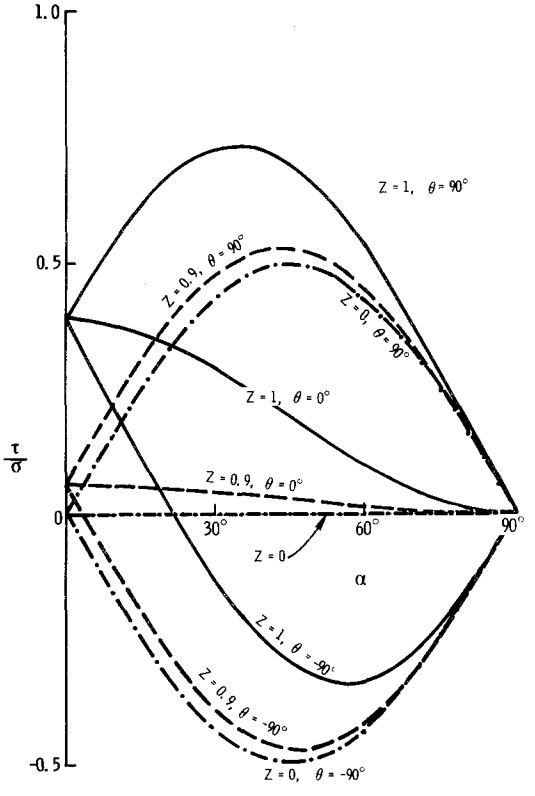

Figure 7 Plot of τ/σ for SMC-30 as a function of α.

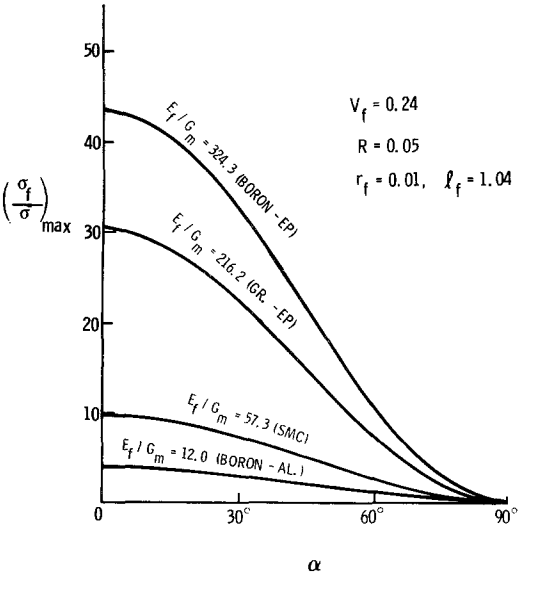

Figure 8 Plot of $\sigma_{f,max}$ as a function of α for different composites.

* This is an interesting possibility, since in [4] the filler material was shown to contribute significantly also to the *stiffness* of the composite.

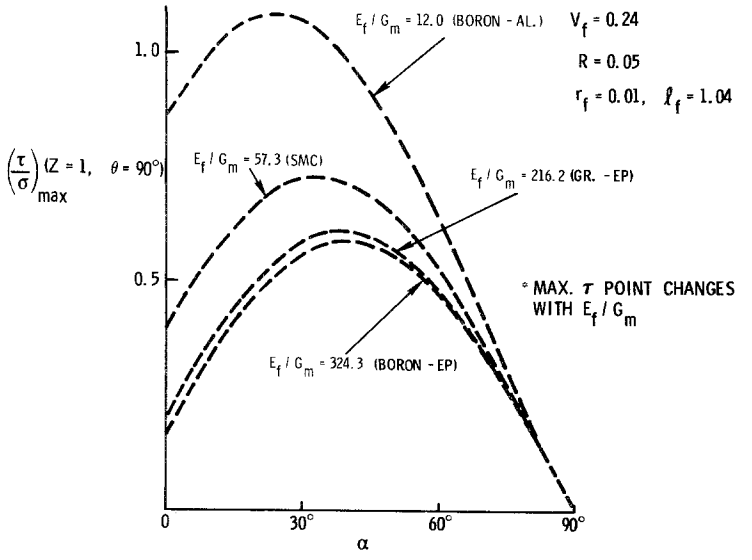

Figure 9 Plot of τ_{max} as a function of α for different composites.

by *fibre pull-out*, *increase* E_f/G_m (again, by modifying the matrix). Unfortunately, such composites usually appear to fail principally by still a third mode, matrix cracking, which this analysis does not treat explicitly (see assumption b). For low fibre-volume fractions, an estimate of the matrix strain might be attempted by noting strain compatibility at the fibre–matrix interface (assumption a), and simply calculating the fibre strain, σ_f/E_f. Strengthening against failure by this third mode, then, is the same as that by fibre breakage – by decreasing E_f/G_m.

In conclusion, it should be emphasized that the results of this report can be used to investigate the theoretical prediction of the incipient tensile strength of randomly oriented chopped-fibre composites, because the fibres then behave nearly linearly to fracture. (The strength may depend on the mode (or modes) of fracture as pointed out above, however, and thus this analysis should be applied only in conjunction with experimental verification.)

Appendix 1

In this appendix, we derive the boundary condition of shear stress τ.

(i) The co-ordinate transformation: in the previous section, we defined two co-ordinate systems (XYZ) and (xyz), whose relationship can be written as

$$\begin{pmatrix} x \\ y \\ z \end{pmatrix} = \begin{bmatrix} 1 & 0 & 0\ 0 \\ 0 & \cos\alpha & -\sin\alpha \\ 0 & \sin\alpha & \cos\alpha \end{bmatrix} \begin{pmatrix} X \\ Y \\ Z \end{pmatrix}. \quad \text{(A1)}$$

Now, let us define another set of the co-ordinate system, $(\bar{x}\bar{y}\bar{z})$ where the $\bar{z}$-axis coincides with z-axis. However, the $\bar{x}$- and $\bar{y}$-axes make an angle θ with the x- and y-axes, respectively, as shown in Fig. 1b; in mathematical notation we can write this as

$$\begin{pmatrix} \bar{x} \\ \bar{y} \\ \bar{z} \end{pmatrix} = \begin{bmatrix} \cos\theta & \sin\theta & 0 \\ -\sin\theta & \cos\theta & 0 \\ 0 & 0 & 1 \end{bmatrix} \begin{pmatrix} x \\ y \\ z \end{pmatrix}. \quad \text{(A2)}$$

Therefore, Equations A1 and A2 give us

$$\begin{pmatrix} \bar{x} \\ \bar{y} \\ \bar{z} \end{pmatrix} = \begin{bmatrix} \cos\theta & \sin\theta\cos\alpha & -\sin\theta\sin\alpha \\ -\sin\theta & \cos\theta\cos\alpha & -\cos\theta\sin\alpha \\ 0 & \sin\alpha & \cos\alpha \end{bmatrix} \begin{pmatrix} X \\ Y \\ Z \end{pmatrix}. \quad \text{(A3)}$$

(ii) Transformation of the stress field: from Equation A3 the transformation matrix $[T]$ is,

$$[T] = \begin{bmatrix} \cos\theta & \sin\theta\cos\alpha & -\sin\theta\sin\alpha \\ -\sin\theta & \cos\theta\cos\alpha & -\cos\theta\sin\alpha \\ 0 & \sin\alpha & \cos\alpha \end{bmatrix}. \quad \text{(A4)}$$

Then

$$\begin{bmatrix} \sigma_{\bar{x}\bar{x}} & \sigma_{\bar{x}\bar{y}} & \sigma_{\bar{x}\bar{z}} \\ \sigma_{\bar{x}\bar{y}} & \sigma_{\bar{y}\bar{y}} & \sigma_{\bar{y}\bar{z}} \\ \sigma_{\bar{x}\bar{z}} & \sigma_{\bar{y}\bar{z}} & \sigma_{\bar{z}\bar{z}} \end{bmatrix} = [T] \begin{bmatrix} 0 & 0 & 0 \\ 0 & 0 & 0 \\ 0 & 0 & \sigma \end{bmatrix} [T]^T \quad \text{(A5)}$$

or

$$\begin{bmatrix} \sigma_{\bar{x}\bar{x}} & \sigma_{\bar{x}\bar{y}} & \sigma_{\bar{x}\bar{z}} \\ \sigma_{\bar{x}\bar{y}} & \sigma_{\bar{y}\bar{y}} & \sigma_{\bar{y}\bar{z}} \\ \sigma_{\bar{x}\bar{z}} & \sigma_{\bar{y}\bar{z}} & \sigma_{\bar{z}\bar{z}} \end{bmatrix} = \sigma \begin{bmatrix} \sin^2\theta \sin^2\alpha & \sin\theta \cos\theta \sin^2\alpha & -\sin\theta \sin\alpha \cos\alpha \\ \sin\theta \cos\theta \sin^2\alpha & \cos^2\theta \sin^2\alpha & -\cos\theta \sin\alpha \cos\alpha \\ -\sin\theta \sin\alpha \cos\alpha & -\cos\theta \sin\alpha \cos\alpha & \cos^2\alpha \end{bmatrix}. \quad \text{(A6)}$$

We are only interested in

$$\sigma_{\bar{x}\bar{z}} = -\sigma \sin\theta \sin\alpha \cos\alpha. \quad \text{(A7)}$$

Therefore,

$$\tau = -\sigma \sin\theta \sin\alpha \cos\alpha \quad \text{at } z = 0. \quad \text{(A8)}$$

Appendix 2

For sheet moulding compounds, customarily 30% by weight polyester resin is used. The rest contains chopped-glass fibres as reinforcement and calcium carbonate particles as fillers. The numerical number after SMC indicates the weight percentage of the chopped-glass fibres. Thus, SMC-30 contains 30% polyester, 30% chopped-glass fibres and approximately 40% calcium carbonate (all by weight). The material properties of each ingredient in SMC are given in Table I.

TABLE I

	Polyester	Calcium carbonate	Glass fibre
Young's modulus (GPa)	3.24	41.4	72.0
Poisson's ratio	0.45	0.21	0.22
Specific weight ($KN\,m^{-3}$)	12.0	27.0	24.0

Acknowledgement

The authors wish to express their thanks to Ms Lisa Riley for the numerical calculation, and to J. William Justusson for his constructive criticism and for pointing out how, depending on the failure mode, the elastic characteristics might be altered to increase the composite strength.

References

1. B. W. ROSEN, "Fibre Composite Materials" (American Society for Metals, Metals Park, Ohio, 1964) Ch. 3.
2. M. A. EISENBERG, "Theory of Fabrication-Induced Anisotropy of Chopped-Fibre/Resin Panels", General Motors Research Laboratories Publication GMR-2633, February (1978).
3. G. J. WENG and C. T. SUN, "Effects of Fibre Length on Elastic Moduli of Randomly-Oriented Chopped-Fibre Composites", presented at the Fifth American Society for Testing and Materials (ASTM) Conference on Composite Materials: Testing and Design, New Orleans, 20–22 March (1978) (ASTM STP (Special Technical Publication) 674, 1979) p. 149.
4. D. C. CHANG and G. J. WENG, "Effective Stiffness of Randomly-Oriented Chopped-Fibre Composites", General Motors Research Laboratories Publication GMR-354, October (1978).

Received 3 May and accepted 29 August 1979.